

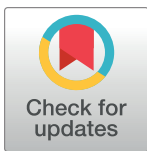
RESEARCH ARTICLE

Creating cell-specific computational models of stem cell-derived cardiomyocytes using optical experiments

Janice Yang¹, Neil J. Daily², Taylor K. Pullinger¹, Tetsuro Wakatsuki², Eric A. Sobie^{1*}

1 Department of Pharmacological Sciences & Graduate School of Biomedical Sciences, Icahn School of Medicine at Mount Sinai, New York, New York, United States of America, **2** InvivoSciences Inc., Madison, Wisconsin, United States of America

* eric.sobie@mssm.edu



Abstract

Human induced pluripotent stem cell-derived cardiomyocytes (iPSC-CMs) have gained traction as a powerful model in cardiac disease and therapeutics research, since iPSCs are self-renewing and can be derived from healthy and diseased patients without invasive surgery. However, current iPSC-CM differentiation methods produce cardiomyocytes with immature, fetal-like electrophysiological phenotypes, and the variety of maturation protocols in the literature results in phenotypic differences between labs. Heterogeneity of iPSC donor genetic backgrounds contributes to additional phenotypic variability. Several mathematical models of iPSC-CM electrophysiology have been developed to help to predict cell responses, but these models individually do not capture the phenotypic variability observed in iPSC-CMs. Here, we tackle these limitations by developing a computational pipeline to calibrate cell preparation-specific iPSC-CM electrophysiological parameters. We used the genetic algorithm (GA), a heuristic parameter calibration method, to tune ion channel parameters in a mathematical model of iPSC-CM physiology. To systematically optimize an experimental protocol that generates sufficient data for parameter calibration, we created *in silico* datasets by simulating various protocols applied to a population of models with known conductance variations, and then fitted parameters to those datasets. We found that calibrating to voltage and calcium transient data under 3 varied experimental conditions, including electrical pacing combined with ion channel blockade and changing buffer ion concentrations, improved model parameter estimates and model predictions of unseen channel block responses. This observation also held when the fitted data were normalized, suggesting that normalized fluorescence recordings, which are more accessible and higher throughput than patch clamp recordings, could sufficiently inform conductance parameters. Therefore, this computational pipeline can be applied to different iPSC-CM preparations to determine cell line-specific ion channel properties and understand the mechanisms behind variability in perturbation responses.

OPEN ACCESS

Citation: Yang J, Daily NJ, Pullinger TK, Wakatsuki T, Sobie EA (2024) Creating cell-specific computational models of stem cell-derived cardiomyocytes using optical experiments. PLoS Comput Biol 20(9): e1011806. <https://doi.org/10.1371/journal.pcbi.1011806>

Editor: Jeffrey J. Saucerman, University of Virginia, UNITED STATES OF AMERICA

Received: January 7, 2024

Accepted: August 8, 2024

Published: September 11, 2024

Copyright: © 2024 Yang et al. This is an open access article distributed under the terms of the [Creative Commons Attribution License](https://creativecommons.org/licenses/by/4.0/), which permits unrestricted use, distribution, and reproduction in any medium, provided the original author and source are credited.

Data Availability Statement: All the code used for this study, including running iPSC-CM model simulations, calibrating and validating models, and processing in vitro and in silico data, can be found at <https://github.com/janice-yang/CM-model-calibration>. In vitro iPSC-CM data are provided in Supplementary S5 Fig, and in silico iPSC-CM data can be reproduced using the code from the CM-model-calibration GitHub repository and the conductance parameter adjustments in Supplementary S2 Table.

Funding: Supported by National Institutes of Health grants U01 HL 136297 and R01 HL 167520 (EAS) and R44 HL 139248 (TW). The study was partially supported by NIH training grant T32 HD 075735. The authors acknowledge computational resources and staff expertise provided by Scientific Computing and Data at Mount Sinai, supported by CTSA grant ULTR004419 from NCATS. The funders had no role in study design, data collection and analysis, decision to publish, or preparation of the manuscript.

Competing interests: I have read the journal's policy and the authors of this manuscript have the following competing interests: "Tetsuro Wakatsuki and Neil Daily are employees with an ownership stake in Invivo Sciences. This company received an NIH SBIR grant that partially funded the research described in the study."

Author summary

Many drug treatments or environmental factors can trigger cardiac arrhythmias, which are dangerous and often unpredictable. Human cardiomyocytes derived from donor stem cells have proven to be a promising model for studying these events, but variability in donor genetic background and cell maturation methods, as well as overall immaturity of stem cell-derived cardiomyocytes relative to the adult heart, have hindered reproducibility and reliability of these studies. Mathematical models of these cells can aid in understanding the underlying electrophysiological contributors to this variability, but determining these models' parameters for multiple cell preparations is challenging. In this study, we tackle these limitations by developing a computational method to simultaneously estimate multiple model parameters using data from imaging-based experiments, which can be easily scaled to rapidly characterize multiple cell lines. This method can generate many personalized models of individual cell preparations, improving drug response predictions and revealing specific differences in electrophysiological properties that contribute to variability in cardiac maturity and arrhythmia susceptibility.

Introduction

Human iPSC-derived cardiomyocytes (iPSC-CMs) come from patient cells that have been reprogrammed into pluripotency and subsequently manipulated to differentiate into the cardiac cell lineage. The development of this *in vitro* platform marked a technological breakthrough in cardiac research, and iPSC-CMs are now widely-used in cardiac pharmacology and disease research. iPSCs can be sourced through minimally-invasive procedures, such as skin biopsy or blood draw, and maintained or banked for long periods [1,2]. These properties of iPSC-CMs make them an ideal platform for pharmacological studies and personalized disease modeling [3]. However, electrophysiological variability between iPSC-CM preparations from different cell lines and differentiation methods limit the potential of this platform [4,5].

Even with recent advances in iPSC-CM maturation protocols [6–9], most iPSC-CMs still display embryonic- or neonatal-like cardiac phenotypes, with different AP and CaT shapes compared with adult myocytes. These phenotypic differences, and how they change temporally, can depend on subtle differences in cell culture conditions and the genetic background of the cell donor [4,5,10], which likely contributes to the wide variation observed between studies [4,5]. No standardized procedure currently exists for characterizing iPSC-CM heterogeneity; prior efforts have generally examined a handful of molecular markers [11], used subjective observations of physiology [12,13], or employed specialized methods such as single cell RNA sequencing [14,15]. These factors, and the potential importance of iPSC-CMs as a research platform, highlight the need for automated methods to characterize the cell lines used in each study.

Mathematical models of cardiomyocyte electrophysiology can provide valuable insight into iPSC-CM electrophysiological variability. These models contain parameters describing the ionic currents and fluxes that contribute to the properties of cardiac action potential (AP) and calcium transient (CaT) waveforms. Several models of iPSC-CM physiology exist in the literature [16–23], with the most recent and comprehensive model published by Kernik et al. in 2019, hereon referred to as the “Kernik model” [20]. However, the baseline parameter values in these models are not representative of the electrophysiological heterogeneity observed in iPSC-CMs. Additionally, parameter calibration has often relied on separate patch clamp measurements of each type of current. This process is time-consuming, inaccessible to many

research groups, and often captures the physiology of only the average behavior of the population of cells examined. Methods to simultaneously optimize several or all model parameters using minimal data are under development [24–28]. Recent work on guinea pig ventricular myocyte models [27] and human iPSC-CM models [28] have demonstrated the utility of automated tuning algorithms for improving model parameterization. Similar work has been done at the level of individual ion channels for calibration of channel kinetic parameters [29]. Much of this iPSC-CM model calibration work uses data generated by direct electrophysiological measurements, e.g. from voltage and current clamp recordings. However, these techniques are not as adaptable for high-throughput experiment setups as optical recordings. Optical measurements trade off exact detection for relative fluorescence values, but they require much simpler laboratory setup and techniques and allow for simultaneous voltage and calcium recording [30,31]. Paci et al. first demonstrated that calibrating models to optical recordings of AP and CaT profiles could refine *in silico* populations of iPSC-CMs and predict channel blockade responses [32].

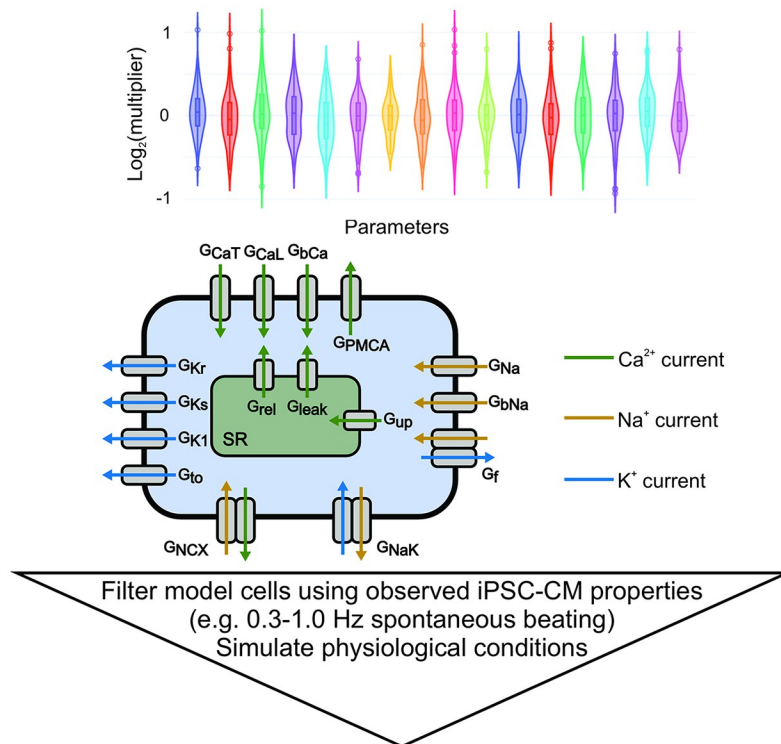
Here we combined these ideas of simultaneous calibration of multiple parameters and optimization of a minimal experimental protocol for generating calibration data. We aimed to create digital twins of iPSC-CM cell preparations from the Kernik iPSC-CM model, thereby connecting observed iPSC-CM electrophysiology with molecular function and mechanisms. We hypothesized that fluorescence readouts of iPSC-CM physiology under varied experimental conditions provide enough information to reveal cellular ion channel properties, which could then be incorporated into the iPSC-CM digital twins. To systematically evaluate various data types and experimental protocols in their ability to inform model parameters, we created a simulated, *in silico* dataset from Kernik model variations with known parameter values. We then developed a computational pipeline which includes: 1) an optimized protocol for fluorescence recordings of iPSC-CM preparations; 2) a genetic algorithm process for calibration of ion channel parameters in iPSC-CM computational model, using the experimental recordings; and 3) validation of the resulting calibrated models by evaluating their predictions on independent, yet physiologically-important, perturbations. We demonstrate the utility of our computational pipeline in generating iPSC-CM digital twins that capture ionic variability and predict cell-specific electrophysiological phenotypes, including drug-induced arrhythmia susceptibility.

Results

Our primary objective was to optimize an experimental protocol for generating sufficient data to calibrate an iPSC-CM mathematical model, taking experimental feasibility and throughput into account. To systematically evaluate how different types of data and experimental conditions impact parameter calibration and model predictions of responses to new conditions or drug treatments, we created a simulated *in silico* dataset, generated from a population of Kernik models with random variations in their 16 maximal conductance parameters (Fig 1A, S1 and S2 Tables, S1 Text). We simulated AP and CaT generated by these model cells under various conditions (S3 Table), and then concatenated these data in various combinations based on the “candidate protocols” we wanted to evaluate. The 16 Kernik model conductance parameters were then calibrated, using a genetic algorithm, to best match the steady state AP and CaT traces from each candidate protocol. These fitted parameters were incorporated into the Kernik model, and the newly-calibrated models were evaluated on their ability to predict the original model cell’s responses to new conditions (outlined in Methods and Fig 1B). Optimizing the experimental protocol using this *in silico* dataset provided 3 major advantages: 1) knowledge of the ground truth parameter values that generated the dataset, so the accuracy of the

A

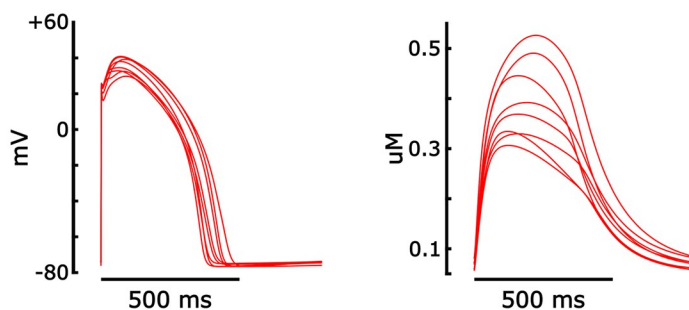
Draw maximal conductance multipliers from a log-normal distribution for 100 Kernik model cells (mean of $\log_2(\text{multiplier}) = 0$, $\sigma = 0.2$)



8 selected Kernik model cells with known conductance parameters, simulated under 19 physiological/pathological conditions:

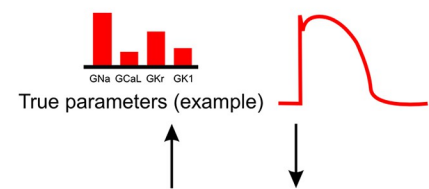
Action potentials (AP):

Calcium transients (CaT):



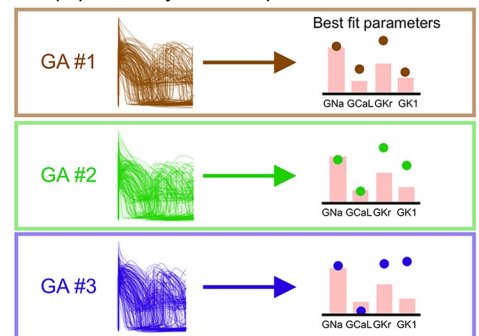
B

1) Input data: Simulated APs, CaTs, or both from 1 Kernik model cell



2) Calibrate model conductance parameters by fitting the input data using the **genetic algorithm (GA).**

Repeating GA runs with different initial populations yields multiple best fit models.



3) Log-normalize calibrated parameter values to corresponding true parameters.

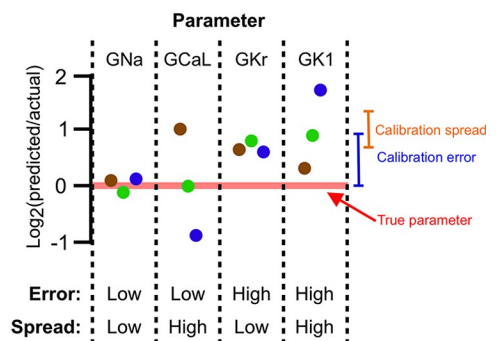


Fig 1. Generation of in silico dataset and calibration pipeline optimization. (A) Schematic of the workflow for creating the *in silico* dataset used to optimize the calibration pipeline. (B) Schematic of the genetic algorithm (GA) parameter calibration process, including 1) the true parameters that generated the input data, 2) example schematics of 3 genetic algorithm runs fitting to the input data, and 3) metrics used to evaluate the resulting fitted parameter values. The genetic algorithm (GA) creates a population of model cells and simulates the same conditions that generated the input data. Then, the error between GA-generated traces and input data is calculated to determine how to modify the population, creating a new population. This process is repeated until the population's errors converge (~20 iterations). Metrics for evaluating calibrations for each model cell: calibration error = $|\log_2(\text{fitted parameter value} / \text{true parameter value})|$; calibration spread = standard deviation between GA runs of $\log_2(\text{fitted parameter value} / \text{true parameter value})$.

<https://doi.org/10.1371/journal.pcbi.1011806.g001>

calibrated parameters can be evaluated, 2) relatively fast and easy simulation of new conditions from the same or additional model cells, in comparison to acquiring new *in vitro* data and cell lines, and 3) generation of various data types using computational methods and data processing, forgoing the need to set up new experiments to collect each data type.

Simultaneously calibrating to AP and CaT data improves model predictions

First, we examined whether AP or CaT recordings alone provided sufficient information for conductance parameter calibration and model predictions. We used simulated recordings from baseline physiological conditions without pacing stimuli (spontaneous APs), and supplied 1) only the AP traces, 2) only the CaT traces, or 3) both (Fig 2A) to the genetic algorithm (GA). The GA calibrates parameters by varying them to create a population of Kernik model cells, then iteratively selecting and modifying individual models that generated AP and CaT traces that best matched the supplied data (outlined in Fig 1B) [33]. We ran the genetic algorithm 10 times per input dataset, with each GA run starting on a different initial population of models. This allowed us to assess whether each input dataset provided enough information to consistently estimate parameter values, even when the initial search space varied.

We evaluated each candidate protocol on parameter calibration accuracy (calibration error) and consistency (calibration spread). Calibration error was represented by the absolute values of calibrated parameters, log-normalized to the corresponding ground truth parameter value, and calibration spread was assessed by calculating the standard deviation (spread) in

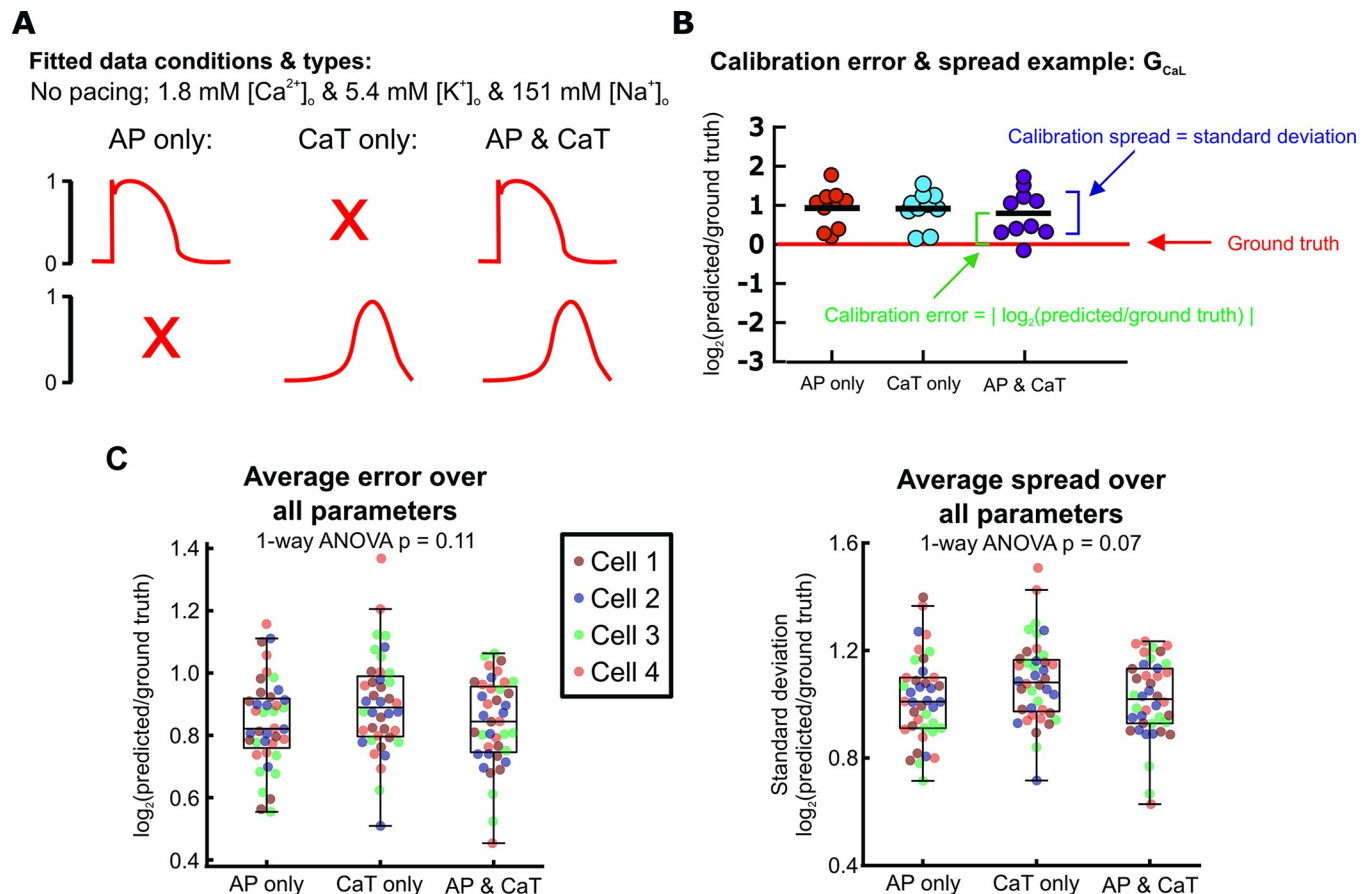


Fig 2. Calibration error and spread remain similar whether only AP, only CaT, or both are included during calibration. (A) Schematic of fitted data types. (B) Example of calibrated parameter values from 10 GA runs per data type for one parameter (G_{CaL}), log-normalized to the ground truth G_{CaL} value of the fitted model cell. Parameter error and spread calculations are visualized. (C) Parameter errors and spreads calculated by comparing calibrated parameters to the corresponding true parameters of 4 model cells from the *in silico* dataset. 10 GA calibration runs were performed per model cell. Each point represents the average error or spread over all 16 fitted parameters from a single genetic algorithm run.

<https://doi.org/10.1371/journal.pcbi.1011806.g002>

log-normalized calibrated parameter values between the 10 runs (Fig 2B). After averaging over all 16 fitted parameters, we found minimal differences in calibration error ($p = 0.11$) or spread ($p = 0.07$) between fitting only voltage, only calcium, or both simultaneously (Fig 2C). From these initial tests, therefore, there appears to be little difference between experimental protocols in how well (or poorly) each can identify model parameters.

We next assessed the calibrated models from each candidate protocol on how well each predicted model cell responses to 30% block of rapid delayed rectifier current I_{Kr} , as this perturbation is both: 1) independent of the conditions used for model calibration and 2) relevant to cardiac pharmacology [34]. With this evaluation (Fig 3A), we found that models fitted to only AP data or only CaT data differed significantly from the ground truth model (Fig 3B and S1 Fig). When both AP and CaT recordings were used simultaneously during parameter calibration, the resulting calibrated models exhibited substantial improvement in their predictions of 30% I_{Kr} block. Therefore, fitting parameters to both AP and CaT traces simultaneously is required for accurate prediction of phenotypes that were not used in the fitting process.

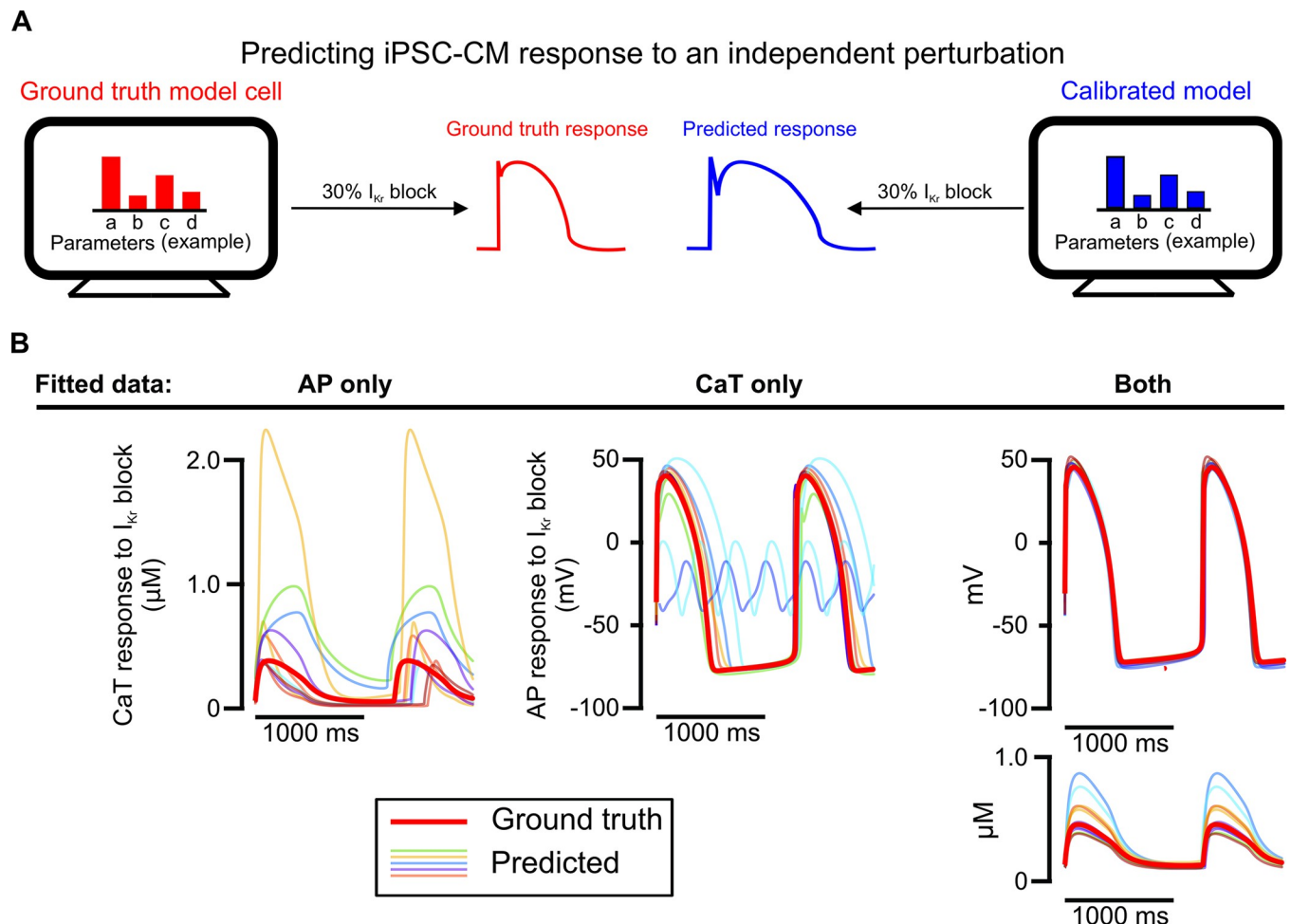


Fig 3. Prediction of iPSC-CM response to an independent perturbation differentiates the models calibrated to AP and CaT simultaneously from those calibrated to single traces. (A) Schematic illustrating the evaluation of calibrated models on their ability to predict an independent response. (B) AP and/or CaT responses to 30% I_{Kr} block predicted by 10 calibrated models for one model cell (thinner traces), compared with the true response of the corresponding model cell (thicker red trace).

<https://doi.org/10.1371/journal.pcbi.1011806.g003>

Overall parameter error and spread show minimal change with varied protocol conditions

Next, we explored how varying the number and type of simulated conditions in the candidate protocols affected parameter calibration. AP and CaT recordings were simulated under many conditions that could be produced in an electrophysiology laboratory and constructed candidate protocols from various combinations of these conditions, which included: 1) varied buffer calcium, from hypo- to normal to hyper-calcemic conditions, 2) spontaneous beating and varied pacing rates from 1–2 Hz, 3) varied levels of L-type calcium channel (I_{CaL}) blockade, and 4) a mixture of these conditions (see Methods for details). We also separated these data into shorter protocols, to see if the experimental setup could be further simplified (Fig 4A). Unexpectedly, we found that parameter errors and spread across all 16 maximal conductance parameters did not differ significantly between the protocols with varied cell culture conditions (Fig 4B, $p = 0.814$ and $p = 0.673$, respectively). Additionally, we observed no significant differences in average calibration errors ($p = 0.088$) and spreads ($p = 0.137$) when varying the

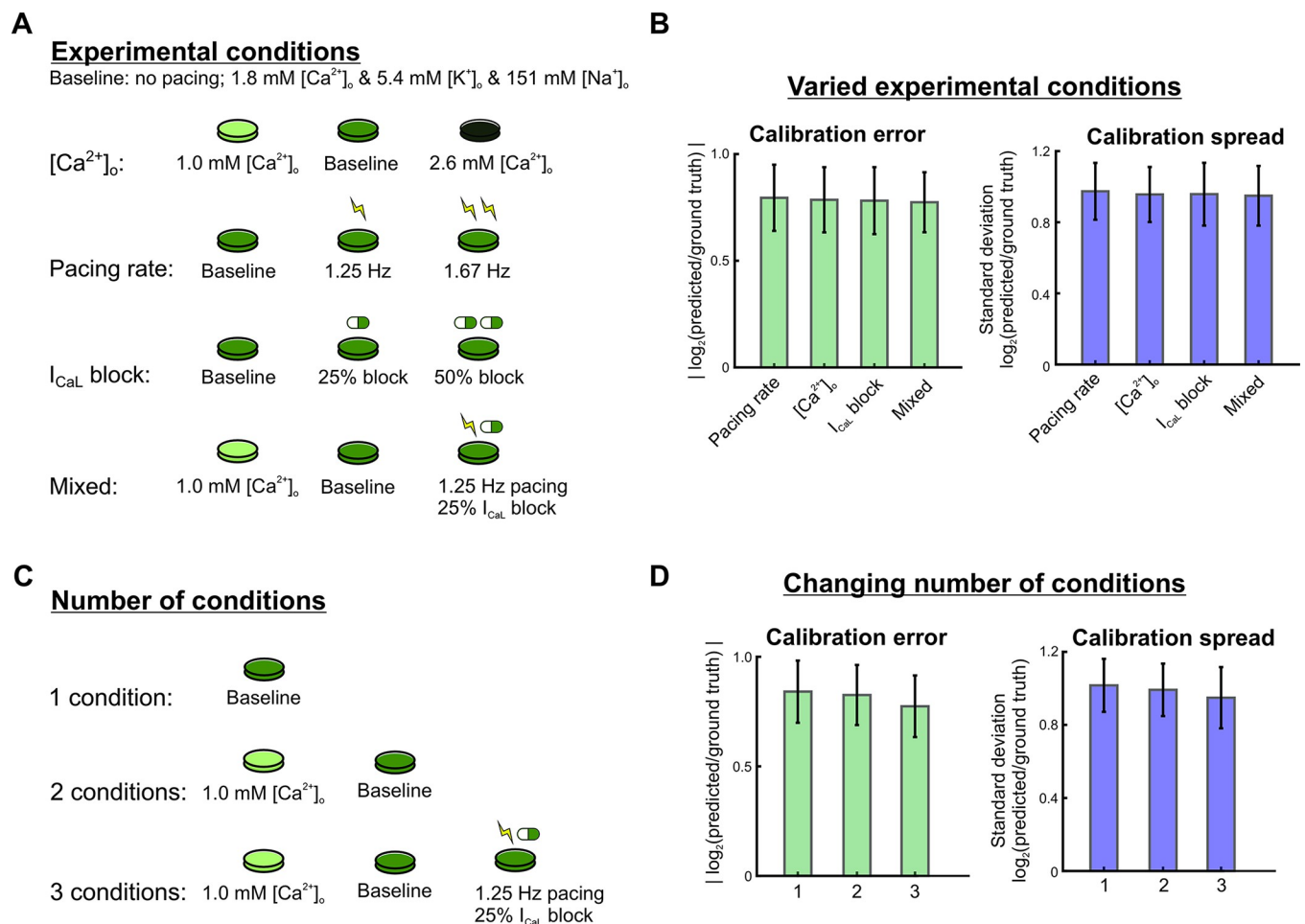


Fig 4. Varying the types and number of experimental conditions has minimal effect on overall calibration error and spread. (A) Schematic of candidate protocols to generate data for model calibration: varied buffer calcium concentration, varied pacing rates, varied I_{CaL} block levels, and a mixture of the 3. (B) Parameter errors and spreads from calibration runs for 4 Kernik model cells (10 GA runs per model cell), using calibration data from each protocol in Fig 4A. Bar plots show the mean calibration errors and spreads over all 16 fitted parameters from all 40 calibration runs. Error bars represent standard deviations over these runs. (C) Schematic of candidate protocols to generate data for model calibration: combinations of 1, 2, or 3 parts of the mixed condition protocol. (D) Parameter errors and spreads from calibration runs for 4 Kernik model cells (10 GA runs per model cell), using calibration data from each protocol in Fig 4B.

<https://doi.org/10.1371/journal.pcbi.1011806.g004>

number of conditions in the protocol (Fig 4C). Similar findings were observed when evaluating different combinations of these experimental conditions (S2 Fig).

A readily-achievable 3-condition protocol improves predictions of I_{Kr} block response

As with the results shown in Fig 3, we assessed how well calibrated models predicted the response to I_{Kr} block, and we found that accuracy depended strongly on the experimental conditions simulated in each candidate protocol (sample AP traces shown in Fig 5A). Out of the protocols using 3 experimental conditions in Fig 4A, the mixed-conditions protocol generated calibrated models with the most accurate predictions of changes in APs with 30% I_{Kr} block, compared with protocols which varied only the buffer calcium, pacing rates, or I_{CaL} blockade (Fig 5B–5C). When evaluating whether a shorter version of this protocol could produce

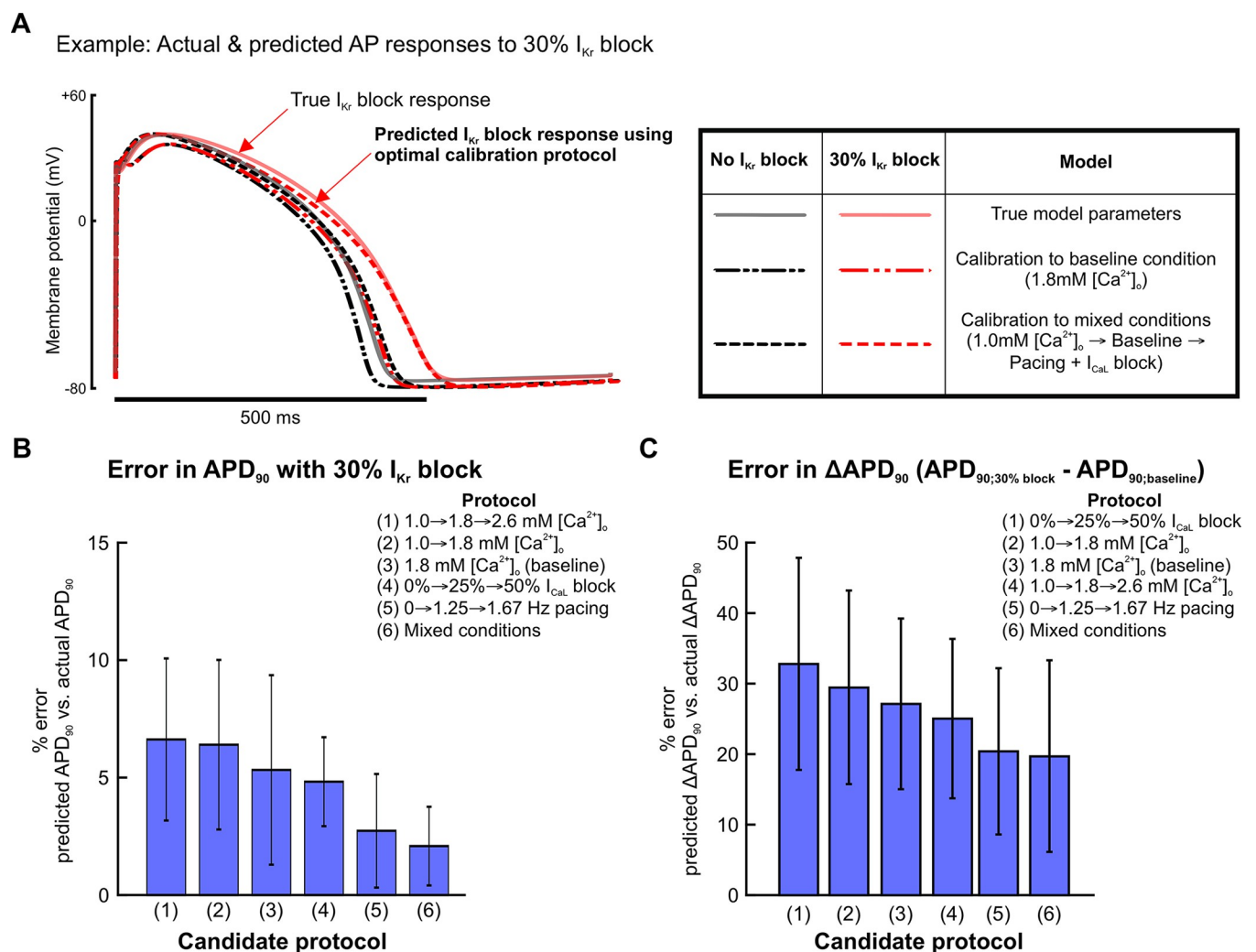


Fig 5. Calibrating parameters to data from the mixed condition protocol improves model predictions of I_{Kr} block response. (A) Examples of simulated steady state APs from baseline (black traces) and 30% I_{Kr} block (red traces) conditions, using the ground truth model cell (solid) and predicted models (dashed). Protocols used for calibration are indicated in the table on the right. (B) Percent error in calibrated model predictions of APD_{90} values at 30% I_{Kr} block. Bars represent means over 10 calibration runs, and error bars represent standard deviations from those same calibration runs. APD_{90} values were normalized to corresponding AP amplitudes before calculating percent error. (C) Percent error in calibrated model predictions of change in APD_{90} (ΔAPD_{90}) between baseline and 30% I_{Kr} block. APD_{90} values were normalized to corresponding AP amplitudes before calculating percent error.

<https://doi.org/10.1371/journal.pcbi.1011806.g005>

equally predictive models, the full protocol with all 3 conditions outperformed protocols with 1 or 2 of the conditions (Fig 5B–5C). These data suggest that an optimal experimental protocol for iPSC-CM model parameter calibration should include voltage and calcium transient fluorescence recordings under at least 3 varieties of cell culture condition changes or perturbations. Of note, this supports our hypothesis that data from iPSC-CMs under a variety of conditions provides sufficient parameter identification to generate predictive models for pharmacological applications.

Normalized fluorescence recordings sufficiently inform parameter calibration

Fluorescence recordings generally detect relative changes and do not provide absolute levels of voltage and calcium. Fluorescent dyes can be calibrated [35,36], and patch clamp can detect true transmembrane potentials, but these are more challenging and lower-throughput techniques compared with straightforward fluorescence recordings. To assess the potential implications for parameter identification, we compared two versions of simulated recordings obtained with our optimized protocol: 1) unscaled (original) *in silico* data, representing patch clamp and calibrated calcium measurements, and 2) normalized versions of the same waveforms, representing simpler fluorescent recordings (Fig 6A).

Parameter calibration accuracy and consistency did not differ significantly when comparing calibrated models from the original data with those from the corresponding normalized data (Fig 6B). Notably, calibrated models from these two data types also performed similarly when evaluating predictions of 30% I_{Kr} block response (Fig 6C). This suggests that fluorescence voltage and calcium recordings from our optimized protocol conditions provide sufficient information to calibrate predictive models. In addition, we ran similar evaluations in which we replaced 30% I_{Kr} block with 30% block of I_{K1} , since this inwardly-rectifying current contributed to iPSC-CM diastolic potential. We suspected that, for these predictions, removing the exact membrane potential information would decrease predictive accuracy. In addition, we ran similar evaluations replacing I_{Kr} block with 30% I_{K1} block, since I_{K1} contributes to the resting membrane potential in iPSC-CMs. We anticipated that removing exact membrane potential information would decrease prediction accuracy in models calibrated to normalized data, and tried to determine whether recordings from multiple conditions would help to recover prediction accuracy. Surprisingly, the majority of calibrated models from normalized data predicted I_{K1} block response with high accuracy, similar to that of the calibrated models from the original data and greatly improved compared with calibrated models from more rudimentary protocols (S3 Fig). This further increased our confidence in using normalized, or optical, AP and CaT recordings for our calibration setup.

Calibrated models predict variability in arrhythmia susceptibility *in silico*

The primary goal of optimizing a computational pipeline for model calibration is to create cell preparation-specific models that can predict variability in phenotypes, particularly arrhythmia susceptibility, between iPSC-CM lines. To assess the ability of our optimized protocol to predict cell line-specific arrhythmia susceptibility, we calculated the lowest level of I_{Kr} block (i.e. highest % I_{Kr}) that induced arrhythmia dynamics (afterdepolarizations, Torsades de Pointes, alternans, beating cessation, or tachycardia) in the same 4 Kernik model cells from our *in silico* dataset. These calculations defined an “ I_{Kr} block tolerance threshold” for each of the 4 model cells (Fig 7A), ranging from 37% I_{Kr} block (highest susceptibility) to 62% I_{Kr} block (highest tolerance) (Fig 7C).

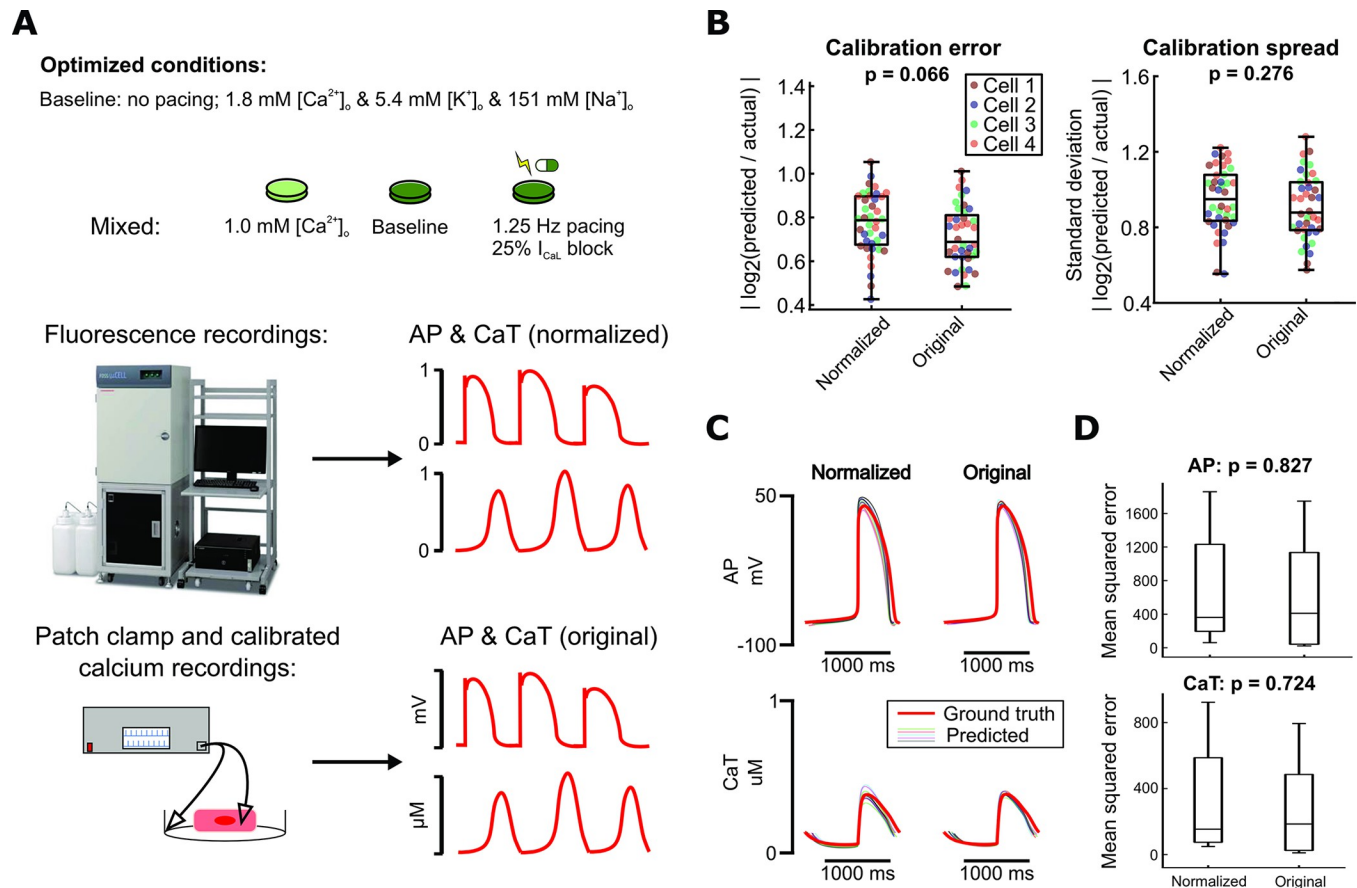


Fig 6. Normalization of calibration data does not significantly affect model calibration results. (A) Schematic of optimized experimental conditions, normalization of simulated data used to represent fluorescence recordings, and original simulated data used to represent more precise measurement modalities. Photo courtesy of Hamamatsu Photonics K.K. (B) Parameter errors and spreads from calibration runs on data from 4 Kernik model cells (10 GA runs per model cell), using either normalized or original data for calibration. Each point represents the average error or spread over all fitted parameters. (C) For 1 model cell: Predicted AP and CaT responses to 30% I_{Kr} block (thinner traces) from each set of calibrations, compared to the true response of the model cell (thicker red trace). (D) For the same model cell as in (C): Mean squared errors between data points in the predicted traces (simulated using calibrated models) and the actual model cell's traces, for simulations under 30% I_{Kr} block.

<https://doi.org/10.1371/journal.pcbi.1011806.g006>

Predicted I_{Kr} block tolerance thresholds were also calculated for the calibrated models generated by our computational pipeline. These predicted thresholds were assessed against the ground truth threshold of the model cell. Calibrated models from our computational pipeline predicted I_{Kr} block thresholds with high accuracy and consistency, with similar error and spread as models calibrated to corresponding non-normalized recordings (Fig 7B). The aggregated calibrated models also predicted relative arrhythmia susceptibility of the 4 model cells, as shown by a significant positive correlation between ground truth and predicted I_{Kr} block thresholds in Fig 7C. Additionally, there was no correlation between the model cell's true I_{Kr} block threshold and its associated calibrated models' prediction error, suggesting that the accuracy of these predictions would not be affected by variability in arrhythmia susceptibility between iPSC-CM preparations (Fig 7D).

Optimized model calibration process constrains key ionic parameters

Throughout the protocol optimization process, we observed that while calibration error and spread largely remained constant when averaged over all fitted parameters, certain individual

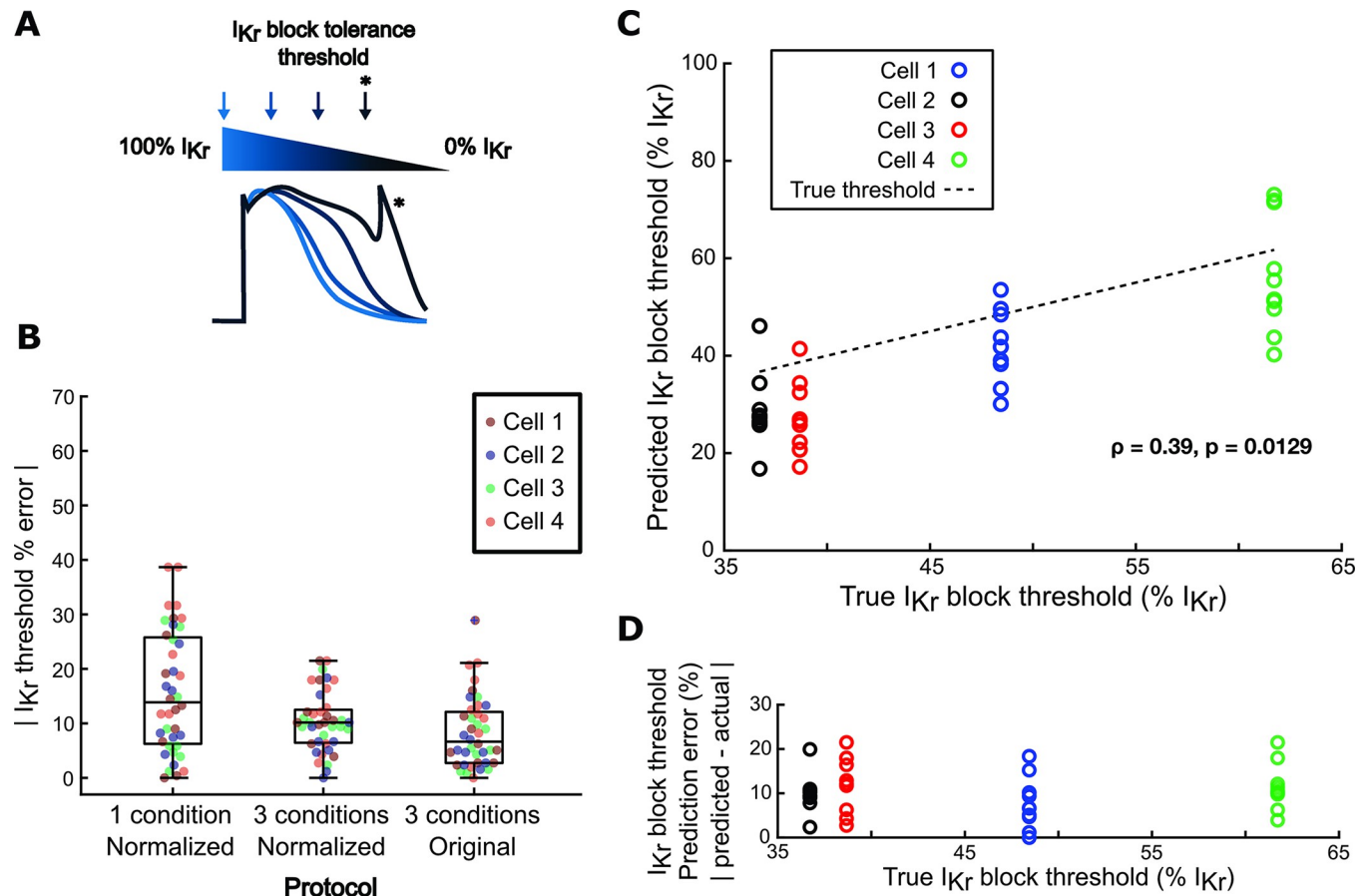


Fig 7. Models generated by the optimized calibration pipeline predict cell-specific arrhythmia susceptibility. (A) Schematic of calculation of I_{Kr} block tolerance threshold. (B) Errors in predictions of I_{Kr} block tolerance threshold, comparing calibrated models from 3 protocols: 1) normalized AP and CaT recordings from a single physiological condition; 2) normalized AP and CaT recordings from the optimized, 3-condition protocol; and 3) non-normalized AP and CaT recordings from the optimized protocol. Each point represents the I_{Kr} block threshold error from 1 calibrated model, and data for 40 calibrations are shown (4 model cells x 10 GA runs per model cell). (C) Correlation between true I_{Kr} block threshold of model cells and their corresponding calibrated models' predicted I_{Kr} block thresholds. (D) Correlation between true I_{Kr} block threshold of model cells and their corresponding calibrated models' I_{Kr} block threshold prediction error.

<https://doi.org/10.1371/journal.pcbi.1011806.g007>

parameters consistently showed low calibration spread (e.g. G_{Kr} , G_{NaK}) or high calibration spread (e.g. G_{rel} , G_{CaT}) (S4 Fig). Thus, we hypothesized that our calibration method only needs to tightly constrain a few key parameters, tolerating inaccuracy or variation in less important parameters while still generating highly predictive calibrated models. To determine whether normalized data from the optimized protocol constrains the parameters that play the largest roles in determining AP and CaT morphology, we analyzed the relationship between parameter calibration accuracy and consistency with the Kernik model's sensitivity to parameter changes. We used multivariable regression to determine how the 16 calibrated model parameters affect relevant phenotypes such as AP duration, CaT amplitude, and I_{Kr} block threshold (Fig 8A) [37]. The resulting model coefficients represent the magnitude and direction of the effect of changes in the corresponding parameter on the modeled phenotype (Fig 8A–8C). The most important parameters depended on which model output was considered (Fig 8A–8C), but parameters that appeared frequently included rapid delayed rectifier K^+ conductance (G_{Kr}), L-type Ca^{2+} conductance (G_{CaL}), Na^+ conductance (G_{Na}), inward rectifier K^+ conductance (G_{K1}), and Na^+/K^+ pump conductance (G_{NaK}).

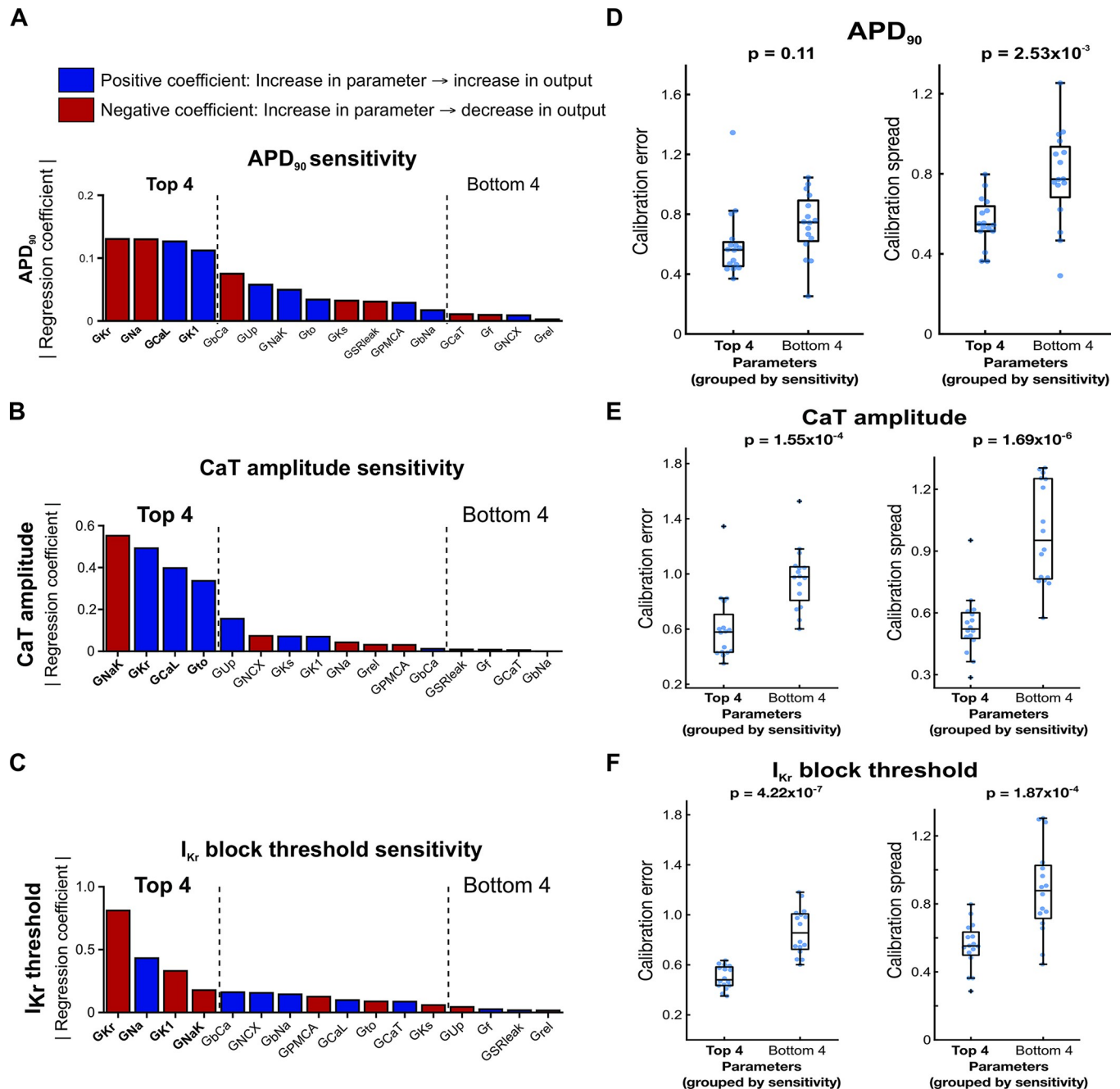


Fig 8. Highly sensitive conductance parameters are well-constrained by the optimized calibration pipeline. (A–C) Regression coefficient magnitudes for each Kernik model maximal conductance parameter's contribution to (A) APD₉₀, (B) CaT amplitude, and (C) I_{Kr} block threshold. Blue bars indicate positive coefficients, and red bars indicate negative coefficients. The top 4 and bottom 4 parameters, ranked by regression coefficient magnitude, are bolded and indicated with black dashed lines. (D–F) Distributions of parameter calibration errors (left) and calibration spread (right) from the optimized calibration pipeline, with parameters grouped into the top 4 and bottom 4 regression coefficient magnitudes for (D) APD₉₀, (E) CaT amplitude, and (F) I_{Kr} block threshold. Each blue dot represents the calibration error or spread value for 1 parameter from calibrations on one model cell (4 parameters per group x 4 model cells = 16 points).

<https://doi.org/10.1371/journal.pcbi.1011806.g008>

We then grouped the parameters into the highest and lowest regression coefficient magnitudes for each phenotype, and assessed calibration errors and calibration spreads from the optimized calibration protocol within those groups. The 4 parameters with highest regression

coefficient magnitudes for CaT amplitude and I_{Kr} block threshold showed significantly lower average calibration error and spread compared with the 4 parameters with the lowest regression coefficient magnitudes (Fig 8E–8F). Accordingly, the optimized calibration protocol displayed significant improvement over most other candidate protocols in predictions of CaT amplitude and I_{Kr} block threshold. We saw similar results when examining calibration errors and spreads in parameters grouped by APD₉₀ sensitivity, though the difference in calibration errors was not statistically significant (Fig 8D). These results suggest that our optimized computational pipeline does constrain the key Kernik model conductance parameters needed to generate predictive models.

Validation of optimized computational pipeline on *in vitro* iPSC-CM recordings

After optimizing our computational pipeline using *in silico* data where the ground truth model parameter values were known, we assessed whether our pipeline could still generate predictive models using *in vitro* data. S5 Fig contains all available *in vitro* iPSC-CM AP and CaT traces under various experimental conditions. We applied the computational pipeline to normalized fluorescence AP and CaT recordings from one iPSC-CM cell line under combinations of the following conditions: 1) low buffer calcium (1.0 mM) with 1 Hz pacing, 2) physiological buffer calcium (1.8 mM) with 1 Hz pacing, and 3) physiological buffer calcium with 1.25 Hz pacing. Fig 9A outlines the data processing and normalization procedures performed on the fluorescence recordings prior to model calibration. Recordings from a separate condition (1.0 mM buffer calcium with 2 Hz pacing) were left out from model calibration, so they could be used to independently evaluate predictions generated by the calibrated model.

Calibrating the model conductances using data from only one of these conditions resulted in unconstrained conductance values and highly variable predictions of response to the left-out validation data (Fig 9B). Including data from 2 additional, mixed conditions significantly improved consistency of key conductance parameter calibrations (Fig 9C). When these calibrated parameters were incorporated into the Kernik model and the cell line's response to a new condition was predicted, we found that models calibrated to recordings from 3 conditions substantially outperformed models calibrated to only 1 condition. These results further supported our findings from *in silico* protocol optimization, showing that data from fluorescence voltage and calcium transients under 3 varied conditions can constrain key model parameters and generate predictive, cell preparation-specific models.

Discussion

While the application of iPSC-derived cardiomyocytes to cardiac disease and pharmacology research has grown dramatically in the past decade, intrinsic and extrinsic variability between cell preparations still hinders reproducibility and clinical translation of studies that use these cells. Generic out-of-box mathematical models of iPSC-CMs do not reflect this variability and potentially generate inaccurate predictions when used to simulate pharmacological ion channel effects or genetic variations [24]. In this study, we aimed to overcome these limitations of the iPSC-CM *in vitro* platform and their mathematical models by creating a computational pipeline which can rapidly identify the cell preparation-specific ionic properties contributing to this phenotypic variability. The parameter calibration algorithm we used, a heuristic genetic algorithm, allows for selection of specific parameters of interest or parameter value limits, and is suitable for parallel computing. To determine the feasibility of this approach, we used a model-generated *in silico* dataset to evaluate candidate protocols containing varied data types and experimental conditions. We found an optimized protocol for fluorescence AP and CaT

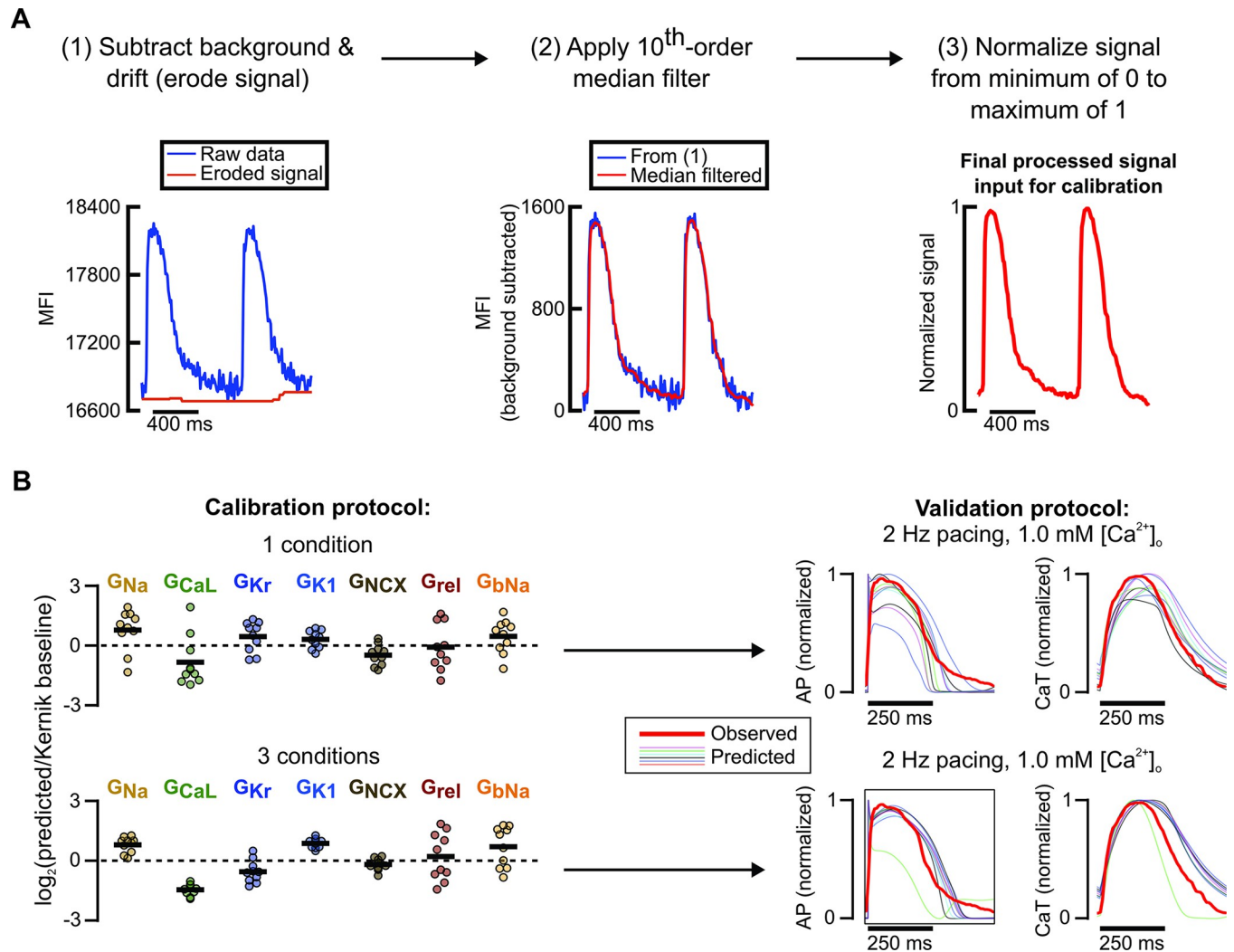


Fig 9. Preliminary model calibrations to *in vitro* data support findings from *in silico* calibrations. (A) Fluorescence recording processing steps in preparation for model calibration pipeline. (B) Top: Resulting calibrated conductance values (left) normalized to Kernik model baseline values (dashed line at 0) and predicted traces under an independent condition (right) when only data from a single condition (1.8 mM [Ca²⁺]_o, 1.25 Hz pacing) is used to fit parameters. Predicted traces (thinner lines) were simulated from 10 models calibrated to recordings from a single sample (thicker red line). Bottom: Resulting calibrated conductance values (left) normalized to Kernik model baseline values (dashed line at 0) and predicted traces under an independent condition (right) when data from a 3-condition protocol (1.0 mM [Ca²⁺]_o, 1 Hz pacing → 1.8 mM [Ca²⁺]_o, 1 Hz pacing → 1.8 mM [Ca²⁺]_o, 1.25 Hz pacing) are used to fit parameters. Predicted traces (thinner lines) were simulated from 10 models calibrated to recordings from a single sample (thicker red line).

<https://doi.org/10.1371/journal.pcbi.1011806.g009>

recordings, consisting of varied buffer calcium concentration, electrical pacing, and I_{CaL} block conditions, which provided enough information to calibrate accurate and predictive cell-specific models, while remaining short in duration and straightforward to acquire. Subsequent model calibrations with an *in vitro* dataset suggested potential flexibility in which specific conditions are selected for the protocol. In our computational pipeline development and subsequent validation, these data were able to inform key ionic contributors, generating calibrated models which accurately and consistently predicted cell-specific responses to both I_{Kr} and I_{K1} block.

Calibration of models of cardiac electrophysiology

Parameter values in computational models of cardiac electrophysiology are often determined by manual fits to voltage and current recordings, often collected under one or few

experimental conditions. This limits the baseline models' ability to represent electrophysiological heterogeneity. Additionally, determination of these baseline parameter values may be affected by selection bias for cells with larger currents, inadequate separation of activation and inactivation kinetics, and inter-laboratory differences in current and voltage clamp protocols [38]. These issues have, in many cases, led researchers to recalibrate the model parameters in attempts to better reflect the behaviors of their specific cardiomyocyte preparations. For example, Potse et al. fitted a reaction-diffusion model of ventricular electrical activity to reproduce phenotypes of patients with heart failure or left branch bundle block [39]. Similarly, Lombardo et al. tuned atrial electrophysiology models for patients undergoing ablation therapy [40] whereas Krogh-Madsen et al. used the genetic algorithm to fit a human ventricular cardiac model to clinical QT interval data [41]. In all three cases, these groups found significant discrepancies between the respective initial models and their final, calibrated, fit-for-purpose models. However, to the best of our knowledge, the experimental data used in virtually all previous cardiomyocyte model calibration research come from voltage clamp, patch clamp, or clinical data. Currently, these data are still difficult to obtain from a large group of patients or cell preparations. More recent work has demonstrated the utility of genetic algorithms and the resulting recalibrated models in prediction of arrhythmic behaviors and drug mechanisms, but these also used complex voltage step protocols to calibrate model parameters [42]. These prior results motivated our search for protocols that could calibrate mathematical models using voltage- and calcium-sensitive fluorescent dye measurements, which are considerably easier to acquire than patch-clamp recordings.

Guiding experimental design for optimal parameter calibration

We considered several factors when optimizing the experimental protocol to generate iPSC-CM data for our computational pipeline: 1) the information that the data would provide for parameter calibration, 2) the complexity of the protocol, and 3) the feasibility of the experiment for broad accessibility and high throughput setups. Since the goal of model calibration is usually to improve the accuracy of model parameterizations and predictions, previous work has largely focused on maximizing the information content of experiments used to fit models [43–45]. In particular, research on cardiac electrophysiology models typically uses complex voltage step protocols that can accurately determine individual ion channel conductances and kinetics [24,46,47]. Here, we emphasize that it is also important to identify adaptable protocols that can be widely adopted. Therefore, we opted to focus on using fluorescence recordings to calibrate model parameters, instead of the usual techniques such as patch clamp. To evaluate different protocols, we created an *in silico* dataset for testing various data combinations in their ability to inform parameter calibration. This approach provided 2 major advantages. First, guided by experimental feasibility and relevance, we were able to simulate iPSC-CM electrophysiology under many combinations of conditions without the time and financial costs associated with *in vitro* experiments. Second, because we knew the ground truth ionic parameter values that produced these AP and CaT traces, we could precisely assess which simulated conditions informed which parameters. We also ran multiple rounds of genetic algorithms on each tested *in silico* protocol, with each round starting from a different initial model population, to assess how consistently each parameter was identified. We used this as a measure of confidence in each parameter estimate.

Just as prior studies have shown that parameter constraint improves when values for more than one output feature are provided [48], we found that calibrating model parameters to fluorescence recordings of AP and CaT traces, as opposed to using only one of the two, resulted in better parameter constraint for some (but not all) parameters. Perhaps more importantly, we

found that calibrating to both outputs simultaneously resulted in significant improvement of the calibrated models' predictions on a new, independent output. This is consistent with prior results which showed that, when translating drug responses across cell types, using multiple electrophysiological features or observations of iPSC-CMs under multiple conditions improved translations [23,49–51]. Similarly, our final optimized protocol included a mixture of 3 experimental conditions. Finally, overall parameter calibration accuracy and consistency, as well as independent predictions of I_{K_r} block response, were similar between the models fitted to normalized data (representing fluorescence data) and those fitted to corresponding non-normalized data (representing patch clamp and calibrated Ca^{2+} transient data). Collectively, these findings support our hypothesis that data from fluorescence recordings under multiple conditions, which are more practical compared with microelectrode or patch clamp recordings, can be used to calibrate predictive models. Notably, several parameters such as the background Ca^{2+} and Na^+ conductances, G_{Ks} , and G_{rel} were rarely constrained by any of the datasets we tested. Our subsequent parameter sensitivity analysis showed that model conductances that strongly affect relevant model outputs tend to be well-constrained by our optimized protocol.

Prediction of cell-specific arrhythmia susceptibility

After calibrating parameters using fluorescence voltage and calcium recordings under a similar set of experimental conditions, we tested the ability of these models to predict conditions that were not used in during the calibration. In particular, we tested the models' ability to predict the pro-arrhythmic effects of I_{K_r} block, given the potential of therapeutics to cause arrhythmias through both on-target and off-target effects [52,53]. This emphasis on prediction rather than parameter identification is consistent with some previous analyses of systems biology models. In an influential paper, Gutenkunst et al. posited that a model that accurately predicts relevant phenotypes even with some parameter value inaccuracies is more useful than a model with high parameter accuracy and consistency, but inaccurate predictions [54]. This suggests that attempting to determine parameter values directly through precise measurements is an inefficient way of optimizing models. Subsequent studies in both cell signaling and cardiac electrophysiology models have demonstrated success in focusing parameter calibrations on optimizing prediction accuracy in place of specific parameter accuracy [25,55,56]. These analyses demonstrate the importance of calibrating models to not only fit available experimental data, but also generate accurate predictions of responses to novel perturbations.

Therefore, while optimizing the computational pipeline, we included a prediction metric in addition to parameter value accuracy and consistency. We created a quantifiable, pharmacologically-relevant measure of cell-specific arrhythmia susceptibility by finding the lowest level of I_{K_r} block that induced arrhythmic dynamics in each Kernik model (*in silico*) or iPSC-CM preparation (*in vitro*), which we termed the " I_{K_r} block tolerance threshold". Calibrated models from our optimized computational pipeline were able to predict this threshold consistently and accurately, with similar error as those from calibrating to the original, non-normalized data. The models calibrated to normalized data were also able to correctly rank the I_{K_r} block arrhythmia susceptibilities of the fitted Kernik model cells, suggesting that the models generated by this pipeline contain enough information to predict cell-specific arrhythmia susceptibilities, despite errors and non-constraint of several smaller conductance parameters.

Limitations and potential directions

The model calibration process developed and optimized in this study can be applied broadly to research that investigates the ionic mechanisms behind iPSC-CM phenotype variability or

predicts differential effects of therapeutics on various iPSC-CM cell lines and preparations. However, phenotypic variability also exists within iPSC-CMs from the same preparation. While it is possible to use fluorescent dyes to record electrophysiology of individual cells, we currently focused our efforts on calibrating models to represent multicellular preparations. Future work could include adapting this computational pipeline to calibrate models representing single cardiomyocytes within an iPSC-CM preparation.

Several conductance parameters fitted in our current pipeline did not contribute significantly to electrophysiological phenotype and responses (e.g. G_F , G_{SRleak} , and G_{rel}), according to our parameter sensitivity analyses. Many of these same parameters were also less accurately constrained by our computational pipeline. While we showed that the resulting calibrated models could accurately predict several major electrophysiology phenotypes and channel block responses, we do not know whether these models could still predict responses that are strongly affected by one or more of the unconstrained parameters. Additionally, other computational models of iPSC-CMs use ionic current contributions that differ from the Kernik model used in this study [17,32,57]. Future calibrations to APs and CaTs simulated from a variety of computational models could help verify whether our current calibration method can tolerate variation in ion current kinetics or contributions, or if further optimization of the calibration protocol is warranted. If improving parameter calibration accuracy and constraint of particular ionic current(s) is found to be necessary for model predictive power, one option would be to replace the conductances with lowest parameter sensitivity regression coefficient magnitudes with representative kinetic parameters, such as time constants or activation gates. If these kinetic parameters are found to impact electrophysiology in a manner that is detectable by the genetic algorithm, their calibrations will likely be more accurate and constrained, generating more precise cell preparation-specific iPSC-CM models.

Conclusions

The optimized model calibration computational pipeline we developed in this study can be applied to ongoing pharmacological and disease studies to understand cell response variability in iPSC-CMs and advance precision medicine. Our pipeline simultaneously fits multiple model parameters to fluorescence voltage and calcium recordings, which are quicker and simpler to acquire than the patch clamp or other more involved electrophysiological techniques used in prior model calibration work. The ability to use fluorescence recordings increases this pipeline's accessibility and throughput compared to prior methods. This unique characteristic makes our computational pipeline suitable for rapid generation of cell-specific models for therapeutic, disease, or population studies. Comparing cell-specific model parameters between iPSC-CM cell lines or to a benchmark, such as an adult cardiac model, would reveal ionic mechanisms behind this variability in iPSC-CM maturation and phenotypes. In addition, the personalized models created by this computational pipeline can simulate patient-specific drug and perturbation responses to quickly predict therapeutic efficacy or drug cardiotoxicity. In future studies, these calibrated iPSC-CM models can inform translation of ionic properties and physiological responses into adult cardiac models, which could, in turn, generate even more accurate, clinically-relevant cardiac electrophysiology phenotype and drug response predictions.

Methods

Simulations of iPSC-CM electrophysiology

In silico simulations of iPSC-CM electrophysiology (e.g. membrane potential, calcium transients, changes in maximal conductances and ionic currents) were carried out in MATLAB

R2020b by solving the ordinary differential equations defined in the Kernik et al. (2019) mathematical model of human iPSC-CMs [20], using the initial conditions listed in [S1 Table](#). In cases where a protocol included cardiomyocyte pacing, electrical stimuli of 60 pA/pF were simulated for a duration of 1 ms at the specified intervals. All simulations were run for 5 minutes, which was sufficient to achieve a steady state using the baseline model and physiological, unperturbed conditions ([S3 Table](#), protocol #19). The voltage and intracellular calcium concentration from the final 5 seconds of each simulation were stored and included in the *in silico* dataset.

***In silico* dataset for optimization of iPSC-CM experimental protocol**

To simulate a heterogeneous set of iPSC-CM cell lines, a “population” of Kernik model cells was created by drawing multiplier factors for each maximal conductance parameter from a log-normal distribution with mean multiplier = 1, spread = 0.2. This population was then simulated under physiological, unperturbed conditions ([S3 Table](#), protocol 19), and filtered for cells which showed a spontaneous beating frequency between 0.3 Hz and 1.0 Hz, nearly matching the automaticity rate range for human iPSC-CMs reported in [58]. Out of the remaining model cells, 4 were randomly selected for simulation under the 19 different conditions, to generate the final *in silico* dataset. The Kernik model’s baseline conductance parameter values and the scaled conductances for these 4 model cells are listed in [S2 Table](#). A list of the various conditions these 4 cells were simulated under can be found in [S3 Table](#). All simulations were run for a 5-minute time span (steady state under physiological buffer conditions, without pacing), and membrane potential and intracellular calcium recordings from the final 5 seconds of these simulations were extracted and stored for the *in silico* dataset. The built-in *interp1* function in MATLAB was used to interpolate these data in equal time steps (0.1 ms). To mimic processed data from fluorescence recordings, we also created “normalized” versions of each dataset by scaling the data from a minimum of 0 to a maximum of 1. This dataset allowed for comparison of conductance parameter estimates produced during model calibration against known ground truth conductance values.

Parameter calibration using the genetic algorithm

The data used for calibrating model parameters included the steady state AP and CaT waves from the previously-generated *in silico* dataset. Individual simulation runs are either included or excluded from the fitting procedure to compare different experimental “candidate protocols”. Rapid delayed rectifier potassium current (I_{Kr}) block conditions were left out from protocol optimization to use for conductance estimate validation. If the candidate protocol consists of more than 1 condition, the final values of membrane potential, intracellular calcium concentration, and other steady state parameters are used as the starting values for the subsequent protocol condition. To determine the optimal protocol for accurate and consistent parameter identification, Kernik model maximal conductance parameters were fitted to *in silico* from each candidate protocol simulated for 4 of the dataset’s model cells, using the genetic algorithm (GA) [24,26]. Briefly, the GA creates a new population of Kernik model cells, each randomly assigned a set of conductance parameter scale factors, and simulates the candidate protocol for each of these model cells. Then, the mean squared error between corresponding data points in the GA-generated trace and the trace from the *in silico* dataset is calculated. The model cells with the lowest errors are retained, while higher-scoring cells have their parameter values altered in the next algorithm iteration. Details about specific GA settings, such as population size and parameter retention/alteration criteria, can be found in [S4 Table](#). This process repeats for 20 iterations, where each new population has a lower average error than the

previous. The parameters of the model cell with the lowest error from the final population are selected as the final calibrated parameter values from that run. Parameter calibrations are conducted 10 times per candidate protocol per model cell, with each of the 10 GA runs starting with a different set of initial model populations. The 10 sets of conductance estimates from each GA run are evaluated on 1) accuracy to the ground truth parameter values of the model cells and 2) ability to predict the model cell's response to a perturbation that was not seen during parameter calibration, such as I_{K_r} block.

***In vitro* iPSC-CM tissue culture and optical recordings**

Human induced pluripotent stem cells (iPSCs) derived from a single cell line were differentiated into cardiomyocytes (iPSC-CMs) by modulating canonical Wnt signaling [59]. The cardiomyocytes were enriched, then combined with cardiac fibroblasts in a ratio of 90% iPSC-CMs to 10% fibroblasts within a collagen-fibrin hydrogel solution (InvivoSciences, Inc., Madison, WI, USA). The engineered heart tissues (EHTs) thus formed were maintained in a serum-free cardiac maintenance medium, supplemented with penicillin and streptomycin (Thermo Fisher Scientific, Waltham, MA, USA), within 96-well micro culture plates (MC-96, InvivoSciences). EHT maintenance was carried out as previously described in relevant literature [60]. Following a five-day remodeling phase, the EHTs underwent further maturation with biphasic constant current electrical stimulations at a frequency of 1Hz for 8 days.

For optical voltage and calcium transient recordings, the EHTs were loaded with Fluovolt (at a dilution of 1:500, Thermo Fisher Scientific), or Cal-520 AM (also at 1:500, AAT Bioquest), along with PowerLoad (Thermo Fisher Scientific), by incubating them for one hour in Tyrode's solution. This solution was prepared with either 1.0 mM or 1.8 mM $[Ca^{2+}]$. Following the removal of the dyes, the solution was pH adjusted to 7.4 and warmed, and Tyrode's solution with the corresponding calcium concentration was reintroduced to aid in recovery from dye loading stress over a 30-minute period. The EHTs were then paced at frequencies of 1.0 Hz, 1.25 Hz, or 2.0 Hz for five minutes. Three replicate samples of each buffer $[Ca^{2+}]$ and pacing frequency were prepared in different wells. The steady-state membrane potential and intracellular calcium transients during this period were recorded using a high-throughput fluorescence plate imager, FDSS/ μ Cell (Hamamatsu Photonics K.K., Japan), utilizing 470nm excitation and 540nm emission at a rate of 125 data points per second. The collected data were analyzed with the iVSurfer software (InvivoSciences), specifically designed for high-throughput waveform data analysis, and one recording per experimental condition was taken for further processing in preparation for model calibration.

Processing of *in vitro* iPSC-CM recordings for the computational pipeline

Fluorescence voltage and calcium recordings were processed in MATLAB with baseline drift subtraction (imerode function), median filtering to remove noise (medfilt1 function), and the same normalization steps as the pseudo-data. Kernik model maximal conductance parameters were fitted to these data using the same workflow as prior fittings to pseudo-data, with the 1.0mM buffer $[Ca^{2+}]$, 2.0Hz pacing data left out for validation.

Supporting information

S1 Fig. Calibrating to both AP and CaT simultaneously improves model predictions of I_{K_r} block response. Predictions of 30% I_{K_r} block response using models calibrated to (A) only AP data, (B) only CaT data, or (C) both AP and CaT data. Ground truth I_{K_r} block responses of the original Kernik model cell are represented by the thicker red traces. Predicted and true I_{K_r} block responses are shown for calibrations using 3 additional Kernik model cells, with similar

findings as those from the representative model cell in the main figures.
(TIF)

S2 Fig. Varying the number of experimental conditions affects model predictions, but not calibration error or spread. (A) Top: Schematic of experimental protocol components: 1—low $[Ca^{2+}]_o$, 2—baseline, 3—baseline with 1.25 Hz pacing and 25% I_{CaL} block. Bottom: Average calibration errors and spreads when calibrating to AP and CaT traces from the indicated protocols, calculated from 40 calibrations (4 model cells x 10 calibrations/cell). Error bars represent standard deviations over these calibrations. (B) I_{Kr} block thresholds predicted using models calibrated to AP and CaT traces from each indicated protocol. The thicker red line indicates the ground truth I_{Kr} block threshold of the Kernik model cell.
(TIF)

S3 Fig. Optimized calibration protocol can generate models that predict I_{K1} block response, despite fitting to normalized data without amplitude information. Predicted (thinner traces) and actual (thicker red trace) AP and CaT responses to blockade of 15% of the I_{K1} current. Data for 1 sample model cell is shown. Predicted traces were simulated using models calibrated with (left to right, 10 calibrations each): 1) only AP data from a single baseline physiological condition; 2) only CaT data from the baseline condition; 3) both AP & CaT data from the baseline condition; 4) normalized AP & CaT data from the optimized calibration protocol; and 5) original, absolute AP and CaT values from the optimized calibration protocol.
(TIF)

S4 Fig. Parameter sensitivities correlate with parameter constraint in most candidate calibration protocols. Plots of calibration spreads for selected conductance parameters: the top and bottom 4 parameters according to I_{Kr} block threshold sensitivity. Results from 4 candidate protocols are shown. Each point represents the mean calibration spread over 10 calibrations on *in silico* data from 1 Kernik model cell. All calibrations shown were performed on normalized AP and CaT traces.
(TIF)

S5 Fig. Ensemble averages of normalized fluorescence intensities of FluoVolt and Cal520 traces from engineered heart tissue samples with different calcium concentrations. Twelve samples were divided into four groups, 1mM $[Ca^{2+}]_o$ FluoVolt (NH1-3), 1.8mM $[Ca^{2+}]_o$ FluoVolt (NH4-6), 1mM $[Ca^{2+}]_o$ Cal520 (NH7-9), and 1.8mM $[Ca^{2+}]_o$ Cal520 (NH10-12). Traces (A-D), (E-H), (I-L), and (M-P) were recorded by electrically stimulating at 2.0, 1.25, 1.0, and 0.5 Hz, respectively, and normalized from 0 to 1. Samples used for the analysis were electrically stimulated for 8 days. Three traces in each group were almost overlapping each other, showing reproducible electrophysiology of the samples. (Q) A normalized trace of fluorescence intensities of FluoVolt of an Engineered Heart Tissue with 1.8mM $[Ca^{2+}]_o$ electrically stimulated at 0.5 Hz. There were no spontaneous depolarizations during the recording of this and any other samples used for the analyses.
(TIF)

S1 Table. Initial membrane potential, ion concentrations, channel states of the Kernik model. Initial conditions were taken from the steady state values of a 10 minute simulation of the baseline model in 151 mM $[Na^+]$, 1.8 mM $[Ca^{2+}]$, 5.4 mM $[K^+]$, without stimulus.
(DOCX)

S2 Table. Maximal conductance parameters used to simulate the *in silico* dataset. Conductance parameter names and values of baseline Kernik model (first 2 columns), and the

corresponding multiplier factors used to create the Kernik model cells in the final *in silico* dataset.

(DOCX)

S3 Table. Experimental conditions included in simulated dataset. A list of the various combinations of extracellular ion concentrations, pacing cycle lengths, and/or channel blocks simulated to generate the *in silico* dataset.

(DOCX)

S4 Table. Genetic algorithm settings. The GA search settings used for all model calibrations in this study.

(DOCX)

S1 Text. Glossary of abbreviations and terms used in this study. Expanded abbreviations and definitions of several phrases commonly used throughout this study.

(DOCX)

Author Contributions

Conceptualization: Janice Yang, Taylor K. Pullinger, Tetsuro Wakatsuki, Eric A. Sobie.

Data curation: Neil J. Daily.

Funding acquisition: Tetsuro Wakatsuki.

Investigation: Janice Yang, Neil J. Daily, Taylor K. Pullinger, Tetsuro Wakatsuki, Eric A. Sobie.

Supervision: Eric A. Sobie.

Validation: Janice Yang, Neil J. Daily, Taylor K. Pullinger.

Visualization: Janice Yang.

Writing – original draft: Janice Yang.

Writing – review & editing: Janice Yang, Tetsuro Wakatsuki, Eric A. Sobie.

References

1. Karakikes I, Ameen M, Termglinchan V, Wu JC. Human Induced Pluripotent Stem Cell-Derived Cardiomyocytes: Insights into Molecular, Cellular, and Functional Phenotypes. *Circ Res*. 2015; 117: 80–88. <https://doi.org/10.1161/CIRCRESAHA.117.305365> PMID: 26089365
2. Huang C-Y, Liu C-L, Ting C-Y, Chiu Y-T, Cheng Y-C, Nicholson MW, et al. Human iPSC banking: barriers and opportunities. *J Biomed Sci*. 2019; 26: 87. <https://doi.org/10.1186/s12929-019-0578-x> PMID: 31660969
3. Hnatiuk AP, Briganti F, Staudt DW, Mercola M. Human iPSC modeling of heart disease for drug development. *Cell Chem Biol*. 2021; 28: 271–282. <https://doi.org/10.1016/j.chembiol.2021.02.016> PMID: 33740432
4. Yang J, Argenziano MA, Burgos Angulo M, Bertalovitz A, Beidokhti MN, McDonald TV. Phenotypic Variability in iPSC-Induced Cardiomyocytes and Cardiac Fibroblasts Carrying Diverse LMNA Mutations. *Front Physiol*. 2021; 12: 778982. <https://doi.org/10.3389/fphys.2021.778982> PMID: 34975533
5. Nakagawa M, Ooie T, Ou B, Ichinose M, Takahashi N, Hara M, et al. Gender differences in autonomic modulation of ventricular repolarization in humans. *J Cardiovasc Electrophysiol*. 2005; 16: 278–284. <https://doi.org/10.1046/j.1540-8167.2005.40455.x> PMID: 15817086
6. Ahmed RE, Anzai T, Chanthra N, Uosaki H. A Brief Review of Current Maturation Methods for Human Induced Pluripotent Stem Cells-Derived Cardiomyocytes. *Front Cell Dev Biol*. 2020;8. Available: <https://www.frontiersin.org/article/10.3389/fcell.2020.00178>.

7. Karbassi E, Fenix A, Marchiano S, Muraoka N, Nakamura K, Yang X, et al. Cardiomyocyte maturation: advances in knowledge and implications for regenerative medicine. *Nat Rev Cardiol*. 2020; 17: 341–359. <https://doi.org/10.1038/s41569-019-0331-x> PMID: 32015528
8. James EC, Tomaskovic-Crook E, Crook JM. Bioengineering Clinically Relevant Cardiomyocytes and Cardiac Tissues from Pluripotent Stem Cells. *Int J Mol Sci*. 2021; 22: 3005. <https://doi.org/10.3390/ijms22063005> PMID: 33809429
9. Guo Y, Pu W. Cardiomyocyte Maturation: New Phase in Development. *Circ Res*. 2020; 126: 1086–1106. <https://doi.org/10.1161/CIRCRESAHA.119.315862> PMID: 32271675
10. Mannhardt I, Saleem U, Mosqueira D, Loos MF, Ulmer BM, Lemoine MD, et al. Comparison of 10 Control hPSC Lines for Drug Screening in an Engineered Heart Tissue Format. *Stem Cell Rep*. 2020; 15: 983–998. <https://doi.org/10.1016/j.stemcr.2020.09.002> PMID: 33053362
11. Lauschke K, Volpini L, Liu Y, Vinggaard AM, Hall VJ. A Comparative Assessment of Marker Expression Between Cardiomyocyte Differentiation of Human Induced Pluripotent Stem Cells and the Developing Pig Heart. *Stem Cells Dev*. 2021; 30: 374–385. <https://doi.org/10.1089/scd.2020.0184> PMID: 33599158
12. Yang X, Pabon L, Murry CE. Engineering Adolescence: Maturation of Human Pluripotent Stem Cell-derived Cardiomyocytes. *Circ Res*. 2014; 114: 511–523. <https://doi.org/10.1161/CIRCRESAHA.114.300558> PMID: 24481842
13. Yoshida Y, Yamanaka S. Induced Pluripotent Stem Cells 10 Years Later. *Circ Res*. 2017; 120: 1958–1968. <https://doi.org/10.1161/CIRCRESAHA.117.311080> PMID: 28596174
14. Kannan S, Farid M, Lin BL, Miyamoto M, Kwon C. Transcriptomic entropy benchmarks stem cell-derived cardiomyocyte maturation against endogenous tissue at single cell level. *PLoS Comput Biol*. 2021; 17: e1009305. <https://doi.org/10.1371/journal.pcbi.1009305> PMID: 34534204
15. Grancharova T, Gerbin KA, Rosenberg AB, Roco CM, Arakaki JE, DeLizo CM, et al. A comprehensive analysis of gene expression changes in a high replicate and open-source dataset of differentiating hiPSC-derived cardiomyocytes. *Sci Rep*. 2021; 11: 15845. <https://doi.org/10.1038/s41598-021-94732-1> PMID: 34349150
16. Paci M, Hyttinen J, Aalto-Setälä K, Severi S. Computational models of ventricular- and atrial-like human induced pluripotent stem cell derived cardiomyocytes. *Ann Biomed Eng*. 2013; 41: 2334–2348. <https://doi.org/10.1007/s10439-013-0833-3> PMID: 23722932
17. Koivumäki JT, Naumenko N, Tuomainen T, Takalo J, Oksanen M, Puttonen KA, et al. Structural Immaturity of Human iPSC-Derived Cardiomyocytes: In Silico Investigation of Effects on Function and Disease Modeling. *Front Physiol*. 2018; 9: 80. <https://doi.org/10.3389/fphys.2018.00080> PMID: 29467678
18. Paci M, Pölönen R-P, Cori D, Penttinen K, Aalto-Setälä K, Severi S, et al. Automatic Optimization of an in Silico Model of Human iPSC Derived Cardiomyocytes Recapitulating Calcium Handling Abnormalities. *Front Physiol*. 2018; 9: 709. <https://doi.org/10.3389/fphys.2018.00709> PMID: 29997516
19. Lei CL, Wang K, Clerx M, Johnstone RH, Hortigon-Vinagre MP, Zamora V, et al. Tailoring Mathematical Models to Stem-Cell Derived Cardiomyocyte Lines Can Improve Predictions of Drug-Induced Changes to Their Electrophysiology. *Front Physiol*. 2017; 8: 986. <https://doi.org/10.3389/fphys.2017.00986> PMID: 29311950
20. Kernik DC, Morotti S, Wu H, Garg P, Duff HJ, Kurokawa J, et al. A computational model of induced pluripotent stem-cell derived cardiomyocytes incorporating experimental variability from multiple data sources. *J Physiol*. 2019; 597: 4533–4564. <https://doi.org/10.1113/JP277724> PMID: 31278749
21. Zhang H, Zou B, Yu H, Moretti A, Wang X, Yan W, et al. Modulation of hERG potassium channel gating normalizes action potential duration prolonged by dysfunctional KCNQ1 potassium channel. *Proc Natl Acad Sci*. 2012; 109: 11866–11871. <https://doi.org/10.1073/pnas.1205266109> PMID: 22745159
22. Lemoine MD, Krause T, Koivumäki JT, Prondzynski M, Schulze ML, Girdauskas E, et al. Human Induced Pluripotent Stem Cell-Derived Engineered Heart Tissue as a Sensitive Test System for QT Prolongation and Arrhythmic Triggers. *Circ Arrhythm Electrophysiol*. 2018; 11: e006035. <https://doi.org/10.1161/CIRCEP.117.006035> PMID: 29925535
23. Jæger KH, Wall S, Tveito A. Computational prediction of drug response in short QT syndrome type 1 based on measurements of compound effect in stem cell-derived cardiomyocytes. *PLOS Comput Biol*. 2021; 17: e1008089. <https://doi.org/10.1371/journal.pcbi.1008089> PMID: 33591962
24. Groenendaal W, Ortega FA, Kherlopian AR, Zygmunt AC, Krogh-Madsen T, Christini DJ. Cell-Specific Cardiac Electrophysiology Models. *PLoS Comput Biol*. 2015; 11: e1004242. <https://doi.org/10.1371/journal.pcbi.1004242> PMID: 25928268
25. Dokos S, Lovell NH. Parameter estimation in cardiac ionic models. *Prog Biophys Mol Biol*. 2004; 85: 407–431. <https://doi.org/10.1016/j.pbiomolbio.2004.02.002> PMID: 15142755

26. Syed Z, Vigmond E, Nattel S, Leon LJ. Atrial cell action potential parameter fitting using genetic algorithms. *Med Biol Eng Comput*. 2005; 43: 561–571. <https://doi.org/10.1007/BF02351029> PMID: 16411628
27. Devenyi RA, Ortega FA, Groenendaal W, Krogh-Madsen T, Christini DJ, Sobie EA. Differential roles of two delayed rectifier potassium currents in regulation of ventricular action potential duration and arrhythmia susceptibility. *J Physiol*. 2017; 595: 2301–2317. <https://doi.org/10.1113/JP273191> PMID: 27779762
28. Akwaboah AD, Tsevi B, Yamlome P, Treat JA, Brucal-Hallare M, Cordeiro JM, et al. An in silico hiPSC-Derived Cardiomyocyte Model Built With Genetic Algorithm. *Front Physiol*. 2021; 12: 675867. <https://doi.org/10.3389/fphys.2021.675867> PMID: 34220540
29. Beattie KA, Hill AP, Bardenet R, Cui Y, Vandenberg JI, Gavaghan DJ, et al. Sinusoidal voltage protocols for rapid characterisation of ion channel kinetics. *J Physiol*. 2018; 596: 1813–1828. <https://doi.org/10.1113/JP275733> PMID: 29573276
30. Lee P, Klos M, Bollensdorff C, Hou L, Ewart P, Kamp TJ, et al. Simultaneous Voltage and Calcium Mapping of Genetically Purified Human Induced Pluripotent Stem Cell-Derived Cardiac Myocyte Monolayers. *Circ Res*. 2012; 110: 1556–1563. <https://doi.org/10.1161/CIRCRESAHA.111.262535> PMID: 22570367
31. Han JL, Heinson YW, Chua CJ, Liu W, Entcheva E. CRISPRi gene modulation and all-optical electrophysiology in post-differentiated human iPSC-cardiomyocytes. *Commun Biol*. 2023; 6: 1236. <https://doi.org/10.1038/s42003-023-05627-y> PMID: 38062109
32. Paci M, Passini E, Klimas A, Severi S, Hyttinen J, Rodríguez B, et al. All-Optical Electrophysiology Refines Populations of In Silico Human iPSC-CMs for Drug Evaluation. *Biophys J*. 2020; 118: 2596–2611. <https://doi.org/10.1016/j.bpj.2020.03.018> PMID: 32298635
33. Wang F-S, Chen L-H. Heuristic Optimization. In: Dubitzky W, Wolkenhauer O, Cho K-H, Yokota H, editors. *Encyclopedia of Systems Biology*. New York, NY: Springer; 2013. pp. 885–885. https://doi.org/10.1007/978-1-4419-9863-7_411
34. Carusi A, Burrage K, Rodríguez B. Bridging experiments, models and simulations: an integrative approach to validation in computational cardiac electrophysiology. *Am J Physiol-Heart Circ Physiol*. 2012; 303: H144–H155. <https://doi.org/10.1152/ajpheart.01151.2011> PMID: 22582088
35. Grynkiewicz G, Poenie M, Tsien RY. A new generation of Ca²⁺ indicators with greatly improved fluorescence properties. *J Biol Chem*. 1985; 260: 3440–3450. [https://doi.org/10.1016/S0021-9258\(19\)83641-4](https://doi.org/10.1016/S0021-9258(19)83641-4) PMID: 3838314
36. Bräuner T, Hülser DF, Strasser RJ. Comparative measurements of membrane potentials with micro-electrodes and voltage-sensitive dyes. *Biochim Biophys Acta BBA—Biomembr*. 1984; 771: 208–216. [https://doi.org/10.1016/0005-2736\(84\)90535-2](https://doi.org/10.1016/0005-2736(84)90535-2) PMID: 6704395
37. Sobie EA. Parameter Sensitivity Analysis in Electrophysiological Models Using Multivariable Regression. *Biophys J*. 2009; 96: 1264–1274. <https://doi.org/10.1016/j.bpj.2008.10.056> PMID: 19217846
38. Krogh-Madsen T, Sobie EA, Christini DJ. Improving cardiomyocyte model fidelity and utility via dynamic electrophysiology protocols and optimization algorithms. *J Physiol*. 2016; 594: 2525–2536. <https://doi.org/10.1113/JP270618> PMID: 26661516
39. Potse M, Krause D, Kroon W, Murzilli R, Muzzarelli S, Regoli F, et al. Patient-specific modelling of cardiac electrophysiology in heart-failure patients. *Europace*. 2014; 16: iv56–iv61. <https://doi.org/10.1093/europace/euu257> PMID: 25362171
40. Lombardo DM, Fenton FH, Narayan SM, Rappel W-J. Comparison of Detailed and Simplified Models of Human Atrial Myocytes to Recapitulate Patient Specific Properties. *PLOS Comput Biol*. 2016; 12: e1005060. <https://doi.org/10.1371/journal.pcbi.1005060> PMID: 27494252
41. Krogh-Madsen T, Jacobson AF, Ortega FA, Christini DJ. Global Optimization of Ventricular Myocyte Model to Multi-Variable Objective Improves Predictions of Drug-Induced Torsades de Pointes. *Front Physiol*. 2017; 8. Available: <https://www.frontiersin.org/articles/10.3389/fphys.2017.01059> PMID: 29311985
42. Clark AP, Wei S, Kalola D, Krogh-Madsen T, Christini DJ. An in silico–in vitro pipeline for drug cardiotoxicity screening identifies ionic pro-arrhythmia mechanisms. *Br J Pharmacol*. 2022; 179: 4829–4843. <https://doi.org/10.1111/bph.15915> PMID: 35781252
43. Liepe J, Filippi S, Komorowski M, Stumpf MPH. Maximizing the Information Content of Experiments in Systems Biology. *PLOS Comput Biol*. 2013; 9: e1002888. <https://doi.org/10.1371/journal.pcbi.1002888> PMID: 23382663
44. Chaloner K, Verdinelli I. Bayesian Experimental Design: A Review. *Stat Sci*. 1995; 10: 273–304. <https://doi.org/10.1214/ss/1177009939>

45. Ryan EG, Drovandi CC, McGree JM, Pettitt AN. A Review of Modern Computational Algorithms for Bayesian Optimal Design. *Int Stat Rev.* 2016; 84: 128–154. <https://doi.org/10.1111/insr.12107>
46. Whittaker DG, Clerx M, Lei CL, Christini DJ, Mirams GR. Calibration of ionic and cellular cardiac electrophysiology models. *Wiley Interdiscip Rev Syst Biol Med.* 2020; 12: e1482. <https://doi.org/10.1002/wsbm.1482> PMID: 32084308
47. Lei CL, Clerx M, Beattie KA, Melgari D, Hancox JC, Gavaghan DJ, et al. Rapid Characterization of hERG Channel Kinetics II: Temperature Dependence. *Biophys J.* 2019; 117: 2455–2470. <https://doi.org/10.1016/j.bpj.2019.07.030> PMID: 31451180
48. Sarkar AX, Sobie EA. Regression Analysis for Constraining Free Parameters in Electrophysiological Models of Cardiac Cells. *PLOS Comput Biol.* 2010; 6: e1000914. <https://doi.org/10.1371/journal.pcbi.1000914> PMID: 20824123
49. Gong JQX, Sobie EA. Population-based mechanistic modeling allows for quantitative predictions of drug responses across cell types. *Npj Syst Biol Appl.* 2018; 4: 1–11. <https://doi.org/10.1038/s41540-018-0047-2> PMID: 29507757
50. Tveito A, Jæger KH, Huebsch N, Charrez B, Edwards AG, Wall S, et al. Inversion and computational maturation of drug response using human stem cell derived cardiomyocytes in microphysiological systems. *Sci Rep.* 2018; 8: 17626. <https://doi.org/10.1038/s41598-018-35858-7> PMID: 30514966
51. Morotti S, Liu C, Hegyi B, Ni H, Fogli Iseppa A, Wang L, et al. Quantitative cross-species translators of cardiac myocyte electrophysiology: Model training, experimental validation, and applications. *Sci Adv.* 2021; 7: eabg0927. <https://doi.org/10.1126/sciadv.abg0927> PMID: 34788089
52. Kannankeril PJ, Roden DM, Norris KJ, Whalen SP, George AL, Murray KT. Genetic susceptibility to acquired long QT syndrome: Pharmacologic challenge in first-degree relatives. *Heart Rhythm.* 2005; 2: 134–140. <https://doi.org/10.1016/j.hrthm.2004.10.039> PMID: 15851285
53. Zequn Z, Yujia W, Dingding Q, Jiangfang L. Off-label use of chloroquine, hydroxychloroquine, azithromycin and lopinavir/ritonavir in COVID-19 risks prolonging the QT interval by targeting the hERG channel. *Eur J Pharmacol.* 2021; 893: 173813. <https://doi.org/10.1016/j.ejphar.2020.173813> PMID: 33345848
54. Gutenkunst RN, Waterfall JJ, Casey FP, Brown KS, Myers CR, Sethna JP. Universally Sloppy Parameter Sensitivities in Systems Biology Models. *PLoS Comput Biol.* 2007; 3: e189. <https://doi.org/10.1371/journal.pcbi.0030189> PMID: 17922568
55. Brown KS, Hill CC, Calero GA, Myers CR, Lee KH, Sethna JP, et al. The statistical mechanics of complex signaling networks: nerve growth factor signaling. *Phys Biol.* 2004; 1: 184. <https://doi.org/10.1088/1478-3967/1/3/006> PMID: 16204838
56. Casey FP, Baird D, Feng Q, Gutenkunst RN, Waterfall JJ, Myers CR, et al. Optimal experimental design in an epidermal growth factor receptor signalling and down-regulation model. *IET Syst Biol.* 2007; 1: 190–202. <https://doi.org/10.1049/iet-syb:20060065> PMID: 17591178
57. Paci M, Koivumäki JT, Lu HR, Gallacher DJ, Passini E, Rodríguez B. Comparison of the Simulated Response of Three in Silico Human Stem Cell-Derived Cardiomyocytes Models and in Vitro Data Under 15 Drug Actions. *Front Pharmacol.* 2021; 12: 604713. <https://doi.org/10.3389/fphar.2021.604713> PMID: 33841140
58. Forny C, Sube R, Ertel EA. Contractions of Human-iPSC-derived Cardiomyocyte Syncytia Measured with a Ca-sensitive Fluorescent Dye in Temperature-controlled 384-well Plates. *J Vis Exp JoVE.* 2018; 58290. <https://doi.org/10.3791/58290> PMID: 30394391
59. Lian X, Hsiao C, Wilson G, Zhu K, Hazeltine LB, Azarin SM, et al. Robust cardiomyocyte differentiation from human pluripotent stem cells via temporal modulation of canonical Wnt signaling. *Proc Natl Acad Sci U S A.* 2012; 109: E1848–E1857. <https://doi.org/10.1073/pnas.1200250109> PMID: 22645348
60. Greenberg MJ, Daily NJ, Wang A, Conway MK, Wakatsuki T. Genetic and Tissue Engineering Approaches to Modeling the Mechanics of Human Heart Failure for Drug Discovery. *Front Cardiovasc Med.* 2018;5. Available: <https://www.frontiersin.org/articles/10.3389/fcvm.2018.00120>.